Lubricated contact model for numerical simulations of suspensions

William Chèvremont, Hugues Bodiguel, B. Chareyre

Lubricated contact model for numerical simulations of suspensions

William Chèvremont[a], Hugues Bodiguel[a,*], Bruno Chareyre[b]

[a] *Univ. Grenoble Alpes, CNRS, Grenoble INP, LRP, 38000 Grenoble, France*
[b] *Univ. Grenoble Alpes, CNRS, Grenoble-INP, 3SR, 38000 Grenoble, France*

Abstract

Discrete granular models are a natural choice when simulating dense suspensions, when the small distances between the particles lead to dominant contributions by lubrication and contact forces. In such case one can get rid of the costly resolution of Navier-Stokes equations, using closed form expressions for lubrication terms. However, those terms diverge when two hard spheres approach contact, and there are issues when integrating them directly with the finite precision of floating point calculations. In this paper, we introduce a visco-elasto-plastic interaction model for suspended spheres, which combines lubrication and elastic-frictional contact behaviour depending on surface roughness. An integration scheme is proposed for that model. Unlike earlier methods, the scheme enables an unconditionally stable time-integration of the interactions. The case of perfectly smooth spheres (null roughness), namely, is integrated correctly. The theoretical results are well reproduced in benchmark tests on two-sphere systems: one sphere sedimenting on one other and two spheres in a shear flow. From these benchmark tests, we propose phase diagrams showing the interplay between viscosity, roughness and stiffness. The second test case highlights the origin of non-reversibility particle trajectories. It is controlled by the particle roughness for rigid particles, and by the particle deformation when the capillary number is higher than the relative roughness.

Keywords: suspension, granular, contact, lubrication, friction

*hugues.bodiguel@univ-grenoble-alpes.fr

1. Introduction

Suspensions of solid particles dispersed in a viscous fluid are ubiquitous in natural, industrial as well as biological flows. For dense suspensions, the resistance to flow depends on a combination of frictional contacts between the particles and viscous interactions mediated by the interstitial fluid. Those combined effects might result in non-Newtonian behaviour even for simple cases such as suspensions of monodisperse spheres in a Newtonian fluid [1, 2]. Particle-scale simulation with discrete element methods (DEM) is a way to investigate the intricate micro-scale processes at play in such flow. There are a few caveats in the concrete implementation of a lubricated contact model in DEM though, and coverage of this point in the literature is scarse whereas many other types of interaction model have been analysed in details (see, namely, [3, 4] and other papers by the same author). This paper contributes a robust method.

Several simulation frameworks have yet been developed in relation to suspensions. Direct Numerical Simulations (DNS) using some Navier-Stokes solvers are feasible though computationally demanding. They require a high spatial resolution to resolve the flow between close particles. Regardless of spatial resolution, though, some singularities will not be captured. Those singularities are associated to the divergence at the approach of contact of the so-called *lubrication forces*, i.e. the viscous resistance to relative motion between two immersed particles. The change of distance between two rigid spheres, namely, leads to a resisting normal viscous force which scales like $\dot{u}_n u_n^{-1}$ if u_n is the gap between the solid surfaces. Since getting this resistance from DNS would require to shrink the spatial resolution to virtually 0 when $u_n \to 0$, the models generally incorporate lubrication corrections to include what's beyhond mesh resolution. The approaches coupling DNS with suspended particles include the Force-Coupling Method (FCM)[5, 6], Fictious Domain method (FD)[7] or Smooth Particle Hydrodynamics (SPH) [8, 9].

While the aforementioned methods spend most of the CPU time in resolving the fluid, multiple authors found that the steady-state flow of suspensions could be simulated accurately by leaving the fluid unresolved and introducing only the lubrication terms through closed form expressions. Down to solid fractions of the order of $\phi = 0.2$,

analytical solutions for regular arrays of spheres [10] as well as numerical solutions in three-dimensional disordered systems [11, 12, 13, 14, 15], provide rather accurate predictions of bulk viscosity by taking lubrication as the only form of viscous dissipation. As lubrication forces decrease sharply with distance the pairs farther than one particle diameter, typically, are insignificant and can be safely ignored. It of course leads to much greater computational efficiency. Worth noting, good agreement with experimental data needs to account not only for the repulsion-attraction effects but also for the viscous response to contact shearing [13] and for contact friction [15].

The lubrication effects being pair-wise interactions they fit well in conventional discrete element methods (DEM), which track the motion of interacting particles with an explicit integration scheme [13], and which was adopted for this work.

The aforementioned models share the same closed-form solutions for the lubrication terms overall. However they differ in the way lubrication and solid contact behaviour are combined. It must be noted that in most DEM models a contact is defined when $u_n < 0$. This situation, which corresponds to a small overlap between the geometrical spheres, reflects a deformation near the contact region, following Hertzian models or some linearized form of them. $u_n < 0$ comes in contradiction with the fact that the lubrication forces diverge when $u_n = 0$, which would in principle prevent contacts. A classical argument to resolve the contradiction, supported by empirical facts[16], is that asperities of the solid surfaces can be in contact when there is still a fluid film of finite thickness between the surfaces. Along this line a surface roughness εa (length scale of the asperities, a being the mean sphere radius and ε relative roughness) is introduced in the models such that the normal lubrication force scale like $(u_n + \varepsilon a)^{-1}$ [17, 18, 19, 13], and thus it takes a finite value when a contact is created (i.e. when $u_n = 0$).

Various implementations of this idea have been proposed. Some authors proposed that whenever $u_n \leq 0$ the viscous multiplier be kept constant [17], or that all lubrication terms be dropped [17, 18, 14] and the interaction model replaced by a linear spring-dashpot model (LSD [20], conventional in dry granular models), tuned in order to produce a specific coefficient of restitution. As pointed out by some authors, though, the restitution coefficient as well as the distance at which lubrication is turned off are additional parameters and the results depend on tuning them relatively arbitrarily [14].

Finally, some authors considered that solid contact and lubrication could act simultaneously and be combined in a visco-elasto-plastic (VEP) model. Therein interaction force at a lubricated contact combines an elastic force in response to some surface deflection and a viscous force in response to changes of gap distance. A simple method to define changes of the gap distance is to set it equal to the total deflection $(u_n + \varepsilon a)$ even if $u_n < 0$ [19], as if soft asperities would deform at the surface of otherwise rigid spheres. Another method[13, 15], which we follow overall, is to let the total contact deflection be split in two parts. One part is the change of gap, coming with the flattening of asperities and producing lubrication effects. The other part is an elastic length u_e corresponding to change of shape around the contact (Hertzian scale) under the combined action of contact forces through asperities and lubricating pressure in the gap. The gap is then $u_n + \varepsilon a - u_e$. This model recovers others as special cases if spheres and asperities have distinct stiffness: a low sphere to asperity ratio corresponds to the hard sphere limit, a high ratio corresponds to the hard asperity limit (constant gap).

A potential downside of the VEP models is that the smooth limit ($\varepsilon \to 0^+$) may be difficult to approach. In the hard sphere limit the interaction forces diverge when $(u_n + \varepsilon a) \to 0^+$ (with $u_n < 0$ at contacts), which sets an implicit lower bound to ε. In addition, viscosity dominated regimes when $(u_n + \varepsilon a)$ is small though strictly positive, may cause instabilities with explicit time integration schemes. This is partly regularized by introducing u_e, but then the stiff problem becomes the time integration of u_e in itself. As a matter of fact $\varepsilon < 10^{-2}$ remained untouched overall with VEP models while other methods were applied successfully to $\varepsilon = 10^{-3}$ [18] or $\varepsilon = 0$ [7].

In this paper a model and a time integration method are proposed to alleviate the limitations of previous VEP approaches; namely

- the physical model is free of arbitrary tricks in combining lubrication and solid contact;
- the limits $\varepsilon \to 0$ and/or $(u_n + \varepsilon a) \to 0$ is approached robustly.

The proposed model is based on the assumption that the elastic deformations comes from both the compliance of individual contact asperities and the global compliance

of the solid surface. Robustness is obtained using an implicit time integration of the interaction forces in an otherwise explicit time-stepping algorithm.

The governing equations and the time integration scheme are given in the first part of the paper. In the second part two test cases are presented to assess the robustness of the approach and to identify different regimes by parametric analysis. The first test case is a suspended sphere subjected to gravitational load and bouncing on another, fixed, sphere; the other involves the interaction of two spheres in a sheared fluid. In both cases theoretical solutions exist and are recovered by our model.

2. Governing equations and time integration

The interaction between two immersed spheres is defined as the sum of two contributions from, respectively, direct (repulsive) contact between the solid surfaces and lubrication by the suspending fluid. It is assumed that they both contribute to deform the spheres elastically and that the deformation occurs through, either, a flattening of the surface asperities leading to a change of the interstitial gap u, or a more general deflection of the surface associated to a local change of shape, as if the sphere radii where modified locally by a small distance u_e. For simplicity linear elasticity is assumed for both modes of deformation in what follows. It will lead to a visco-elastic model similar to the *standard linear solid* model, yet with variable viscosity. The approach could be extended to non-linear contact models, such as Hertzian ones, without major difficulty.

In the following, we detail the governing equations of the model. Since time integration only requires the calculations of interaction forces and torques between the two spheres at a given time step and is furthermore not the focus of the present work, we start by presenting these forces and torques. Since they involves intermediate quantities, and in particular the interstitial gap u between the (deformed) surface, their evaluation is not straightforward. In section 2.1, we first detail the normal component of the forces and explain how to efficiently compute the interstitial gap using an implicit scheme. Then, we detail the tangential components in section 2.2. These are more direct as there is no direct coupling with u contrary to the case of normal ones. However, several cases need to be distinguished, depending on the type of contact (no contact,

sticking contact and slipping contact). Time integration is finally described briefly in section 2.3, but is beyond the scope of this paper.

2.1. Normal components

2.1.1. Solid contact

It is assumed that a finite repulsive contact force arises whenever the interstitial gap is less than the size of asperities. For two particles of mean radius $a = (r_1 + r_2)/2$ the normal component of the contact force is taken proportional to the deflection of the asperities, following

$$\mathbf{F}_n^c = -k_n \max(0, \varepsilon a - u)\mathbf{n} \tag{1}$$

where εa defines the characteristic size of the asperities, and ε is termed *relative roughness*. k_n is the normal stiffness of the asperities, and u is the distance between the solid surfaces (not counting the size of asperities). $\mathbf{n}$ is the unit normal of the contact (see figure 1). Here and in the following, subscripts n and s denote normal and shear components of the interactions, respectively. Superscript c and l will be used to distinguish contact and lubrication contributions.

In the elastic regime the tangential component of the contact force is an incrementally linear function of the tangential displacement. The contact model includes a threshold on the magnitude of the shear force following Coulombian friction, as in Cundall and Strack [21]. The shear force thus has to satisfy the inequality:

$$\|\mathbf{F}_s^c\| \leq \mu_m \|\mathbf{F}_n^c\|, \tag{2}$$

where μ_m is the coefficient of contact friction.

2.1.2. Lubrication

The lubrication terms are defined as in Marzougui et al. [13]. They define the viscous resistance to relative motion between particles.

$$\mathbf{F}_n^l = \frac{3}{2}\pi\eta_f a^2 \frac{\dot{u}}{u}\mathbf{n} \tag{3}$$

$$\mathbf{F}_s^l = \frac{\pi\eta_f}{2}\left[-2a + (2a+u)\ln\left(\frac{2a+u}{u}\right)\right]\dot{\mathbf{v}} \tag{4}$$

$$\mathbf{T}_r^l = \pi\eta_f a^3\left(\frac{3}{2} + \frac{63}{500}\frac{u}{a}\right)\ln\left(\frac{a}{u}\right)\boldsymbol{\omega}\times\mathbf{n} \tag{5}$$

$$\mathbf{T}_t^l = \pi\eta_f a^2 u \ln\left(\frac{a}{u}\right)(\boldsymbol{\omega}\cdot\mathbf{n})\mathbf{n} \tag{6}$$

where $\boldsymbol{F}_n^l$, $\boldsymbol{F}_s^l$, $\boldsymbol{T}_r^l$ and $\boldsymbol{T}_t^l$ are respectively normal lubrication force, tangential lubrication force, rolling lubrication torque and twisting lubrication torque. $\mathbf{v}$ is the tangential displacement, ω the spin velocity, and η_f the fluid velocity. The expressions are based on Frankel and Acrivos [22] for the forces and Jeffrey and Onishi [23] for the torques.

Although the above expressions define the lubrication terms for virtually any distance u, they are exact only asymptotically in the limit $u/a \to 0$. In practice, they are computed only for particle pairs within a distance range. The torques (equations 5-6) are computed as long as $u \leq a$. For $u > a$ the direction of the torques switches to the same direction as the relative rotation and thus physical consistency is lost - which justifies the upper bound unambiguously. There normal and shear forces (equations 3-4) are also cut off beyond a certain distance yet there is no simple argument to fix the maximum distance in that case. The cut-off distance is left as a model parameter for now. It will be further examined on the basis of the second test case.

For writing simplicity, prefactors $\nu_n, \nu_t(u)$ are introduced in the expression of forces, such that:

$$\nu_n = \frac{3}{2}\pi\eta_f \tag{7}$$

$$\nu_t(u) = \frac{\pi\eta_f}{2}\left[-2a + (2a+u)\ln\left(\frac{2a+u}{u}\right)\right] \tag{8}$$

$$\mathbf{F}_n^l = \nu_n a^2 \frac{\dot{u}}{u}\mathbf{n} \tag{9}$$

$$\mathbf{F}_s^l = \nu_t(u)\dot{\mathbf{v}} \tag{10}$$

2.1.3. Visco-elastic coupling

Contact and lubrication are combined in a rheological model summarized in figure 1. Three different length appear in the model: the gap between the solid surfaces u, the deflection of surfaces u_e, and finally the change of center-to-center distance with respect to the stress free configuration: $u_n = |\boldsymbol{r}_1 - \boldsymbol{r}_2| - 2a$, with $\boldsymbol{r}_{1,2}$ the positions vectors and $2a$ the sum of radii. The gap u is always positive, u_n and u_e can be positive or negative ($u_e > 0$ when lubrication produces traction between separating bodies). u_n depends only on the particles positions which, in concrete cases, will result from integrating the equations of motion for the particles (which is done independently of the present derivation). A change of the center-to-center distance relative to the stress free configuration implies that either the distance between the surfaces is changing, or the surfaces are deforming, or both. In all cases u_n accumulates the other two displacements and the following equality holds:

$$u_n = u + u_e \tag{11}$$

It is assumed that the lubricating pressure and the contact forces through asperities both contribute to deflect the surfaces by a distance u_e in the normal direction, and that the compliance is defined by a single coefficient of stiffness k_b such that the total normal force $\mathbf{F}_n = \mathbf{F}_n^l + \mathbf{F}_n^c$ and u_e are linearly dependent:

$$\boldsymbol{F}_n = k_b u_e \boldsymbol{n} \tag{12}$$

Combining equations 1, 3 and 12 and projecting in the normal direction $\boldsymbol{n}$ yields the scalar form

$$k_b u_e = -k_n \max(0, \varepsilon a - u) + \nu_n a^2 \frac{\dot{u}}{u} \tag{13}$$

Elimination of u_e using equation 11 yields a differential equation governing the visco-elastic coupling, where u is the only unknown (owing to the fact that u_n results from motion integration). Normalization by the length a and the characteristic visco-

elastic time $\tau = \eta a/k_b$ leads to the dimensionless form

$$(1+\alpha)u^* - u_n^* - \alpha\varepsilon + \frac{\dot{u}^*}{u^*} = 0 \tag{14}$$

$$\alpha(u^*) = \begin{cases} 0 & \text{when} \quad u^* > \varepsilon \quad \text{(no contact)} \\ \dfrac{k_n}{k_b} & \text{when} \quad u^* <= \varepsilon \quad \text{(contact)} \end{cases} \tag{15}$$

Here and in the following "*" is used to denote the dimensionless form of a variable (e.g. $u^* = u/a$). In this paper, k_n/k_b is set equal to 1 at contacts; in other words the stiffness of asperities and the stiffness of the surfaces are taken equal. The numerical scheme is compatible with all positive values.

[Figure 1 about here.]

Tracking the evolution of the interaction with time asks for u integration using equation 14 while continuously updating u_n to reflect particles motion. For this purpose, and in order to insure unconditional stability, an implicit backward Euler method is used. The time derivative of u^* is approximated by

$$\dot{u}^{*+} = \frac{u^{*+} - u^{*-}}{\Delta t^*} + O(\Delta t^*), \tag{16}$$

where Δt^* is the time step normalized by τ, and the exponents "$^-$" and "$^+$" refer to the times at which a quantity is evaluated (the start and the end of the time interval). Using equation 14, we obtain

$$\left(u^{*+}\right)^2 (1+\alpha^+) - u^{*+}\left(u_n^* + \alpha^+\varepsilon - \frac{1}{\Delta t^*}\right) - \frac{u^{*-}}{\Delta t^*} = 0, \tag{17}$$

which is a second order polynomial equation, of positive discriminant. The smallest solution is always negative, hence rejected since the gap u is positive. Finally the updated gap and the associated force are given by

$$u^{*+} = \frac{1}{2(1+\alpha^+)}\left[\left(u_n^* + \alpha^+\varepsilon - \frac{1}{\Delta t^*}\right) + \sqrt{\left(u_n^* + \alpha^+\varepsilon - \frac{1}{\Delta t^*}\right)^2 + 4(1+\alpha^+)\frac{u^{*-}}{\Delta t^*}}\right] \tag{18}$$

$$\boldsymbol{F}_n = k_b a\left(u_n^* - u^{*+}\right). \tag{19}$$

Interestingly, equation 18 remains applicable for every positive value of u and it does not suffer from the singular evolution of lubrication as $u \to 0^+$. This is a key property of the proposed approach.

The function α that is used to write the general solution introduces discontinuous derivatives at the transition between contact and no-contact solutions, and it has to be handled with care. Setting $u^{*+} = \varepsilon$ in equation 17 gives the time delay after which the transition occurs, i.e.

$$t_c^* = \frac{\varepsilon - u^{*-}}{\varepsilon(\varepsilon - u_n)}. \tag{20}$$

Where t_c^* is the dimensionless critical collision time. If t_c^* is positive and the dimensionless time step $\Delta t^* > t_c^*$, a contact transition occurs within the time step. In such a case, we integrate on a fraction of the nominal time-step, noted Δt^*, and starting from an intermediate solution (variables subscripted with i) which correspond to the transition:

$$\left\{ \begin{array}{rcl} u_i^{*-} & = & \varepsilon \\ \Delta t_i^* & = & \Delta t^* - t_c^* \\ \alpha_i^+ & = & 1 - \alpha^+ \end{array} \right. \tag{21}$$

Implementing equation 18 directly would have detrimental effects in terms of accuracy when both u^* and u_n^* are small. This is because with such settings the terms $1/\Delta t^*$ dominate all other terms in equation 18, which leads to a substraction of two nearly equal terms, beyond the accuracy of floating point operations. The algorithm would effectively give $u^* \leq 0$ after some time if a contact pair is compressed permanently. The fact that u^* appears often in a logarithm suggests the change of variable $\xi = \log(u^*)$ to circumvent this accuracy issue. The following equation on ξ now has to be solved:

$$(1 + \alpha^+)\exp(\xi^+) - \left(u_n + \alpha^+\varepsilon - \frac{1}{\Delta t^*}\right) - \frac{\exp(\xi^- - \xi^+)}{\Delta t^*} = 0 \tag{22}$$

This equation can be solved by conventional non-linear solvers, initialized at $\xi^+ = \xi^-$. The bisections method is used in the current implementation.

2.2. Tangential components

The tangential forces are combined in a visco-elastic model as shown in figure 2. Like for the normal part, lubrication and contact act in parallel, and they both contribute

to distord (or to shear) the solid surfaces. Unlike the normal behaviour, described by a single scalar equation, the quantities $\boldsymbol{v}_s, \boldsymbol{v}_e$, and $\boldsymbol{v}$, defining the tangential displacements, are vector quantities. They need to be handled as such to reflect changes in the direction of shearing and rotations of the particle pair. $\boldsymbol{v}_s$ is the geometrical shear displacement, obtained by integrating shear velocity over time. $\boldsymbol{v}_e$ is the elastic part of $\boldsymbol{v}_s$ produced by shearing the particles around a sticking contact area. $\boldsymbol{v}$ is the accumulated plastic slip, i.e. $\boldsymbol{v} = \boldsymbol{v}_s - \boldsymbol{v}_e$. The lubrication forces are activated by plastic slip, assuming that viscous stresses in the interstitial fluid are negligible when the contact sticks.

$\boldsymbol{v}_s$ is always known before computing the tangential interaction. Just like u_n for the normal component it results from motion integration. The gap u can be considered known, too, since it was derived in the previous section independently of the tangential components.

[Figure 2 about here.]

The evolution of the shear components is governed by the system of equations

$$\begin{cases} \boldsymbol{v}_s &= \boldsymbol{v}_e + \boldsymbol{v} \\ \boldsymbol{F}_s &= -k_t \boldsymbol{v}_e = \min\left(\|\boldsymbol{F}_s^c\|, \mu_m \|\boldsymbol{F}_n^c\|\right) \dfrac{\boldsymbol{F}_s^c}{\|\boldsymbol{F}_s^c\|} - \nu_t(u)\dot{\boldsymbol{v}}. \end{cases} \tag{23}$$

The equations express, respectively, the additivity of elastic and plastic displacement, and the force evaluated alternatively in the spring component then in the visco-plastic component. A Coulombian slider accounts for the frictional solid contact (components of force $\boldsymbol{F}_s^c$ and $\boldsymbol{F}_n^c$), and a Newtonian dashpot with u-dependent viscosity reflects lubrication by the fluid. There is no need to integrate the total plastic slip vector $\boldsymbol{v}$ over time in practice since its rate of change suffice to integrate the above equations.

The problem is now solved for the tree possible cases: no contact ($u > \varepsilon a$), sticking elastic contact ($\boldsymbol{v} = 0$), and slipping contact ($\|\boldsymbol{F}_s^c\| = \mu_m \|\boldsymbol{F}_n^c\|$). If there is contact, the force is first evaluated by assuming a sticking regime. Then, if the magnitude of the trial force $\boldsymbol{F}_s^{c*}$ exceeds the frictional threshold, the Coulomb condition is taken into account. Similarly as the normal part, we derive an implicit scheme based on backward Euler approximation for the time derivative, i.e.

$$\dot{\boldsymbol{v}}_e = \frac{\boldsymbol{v}_e^+ - \boldsymbol{v}_e^-}{\Delta t} + O(\Delta t). \tag{24}$$

The three cases are detailed below.

2.2.1. *No contact*

If the normal contact force is null, the shear contact force is also null as a consequence of Coulomb condition. Equations 23 degenerate to a Maxwell-type visco-elastic equation given by

$$-k_t \boldsymbol{v}_e = -\nu_t(u)(\dot{\boldsymbol{v}}_s - \dot{\boldsymbol{v}}_e). \tag{25}$$

Using equation 24 and rearranging yields to

$$\boldsymbol{v}_e^+ = \frac{-\nu_t(u)(\dot{\boldsymbol{v}}_s \Delta t + \boldsymbol{v}_e^-)}{\nu_t(u) + k_t \Delta t} \tag{26}$$

and to

$$\boldsymbol{F}_s^+ = \frac{\nu_t(u)(\boldsymbol{F}_s^- - k_t \dot{\boldsymbol{v}}_s \Delta t)}{\nu_t(u) + k_t \Delta t}. \tag{27}$$

2.2.2. *Sticking contact*

If the contact is sticking over a time interval, the elastic displacement rate is equal to total displacement rate: $\dot{\boldsymbol{v}}_e = \dot{\boldsymbol{v}}_s$ (no slip). The incremental change of $\boldsymbol{v}_e$ can be obtained by direct integration of $\dot{\boldsymbol{v}}_s$ and in this purely elastic regime the force changes linearly with respect to this change, i.e.

$$\boldsymbol{v}_e^+ = \dot{\boldsymbol{v}}_s \Delta t + \boldsymbol{v}_e^-, \tag{28}$$

$$\boldsymbol{F}_s^{e+} = \boldsymbol{F}_s^- - k_t \dot{\boldsymbol{v}}_s \Delta t.. \tag{29}$$

The force obtained herein by assuming no-slip is a *trial* elastic force, which may or may not satisfy Coulomb condition. If it does, then we set simply $\boldsymbol{F}_s^+ = \boldsymbol{F}_s^{e+}$. If it does not then we proceed to the third case (slipping contact) to find a visco-elasto-plastic solution.

2.2.3. *Slipping contact*

The trial elastic force from Eqs. 29 defines the direction of the contact force and of the plastic slip if it occurs. An equivalent form of equations 23 is then

$$-k_t \boldsymbol{v}_e = \mu_m \|\boldsymbol{F}_n^c\| \frac{\boldsymbol{F}_s^{e+}}{\|\boldsymbol{F}_s^{e+}\|} - \nu_t(u)(\dot{\boldsymbol{v}}_s - \dot{\boldsymbol{v}}_e). \tag{30}$$

Using equation. 24, we obtain

$$\boldsymbol{v}_e^+ = \frac{\mu_m \|\boldsymbol{F}_n^c\| \dfrac{\boldsymbol{F}_s^{e+}}{\|\boldsymbol{F}_s^{e+}\|} \Delta t - \nu_t(u)\left(\dot{\boldsymbol{v}}_s \Delta t + \boldsymbol{v}_e^-\right)}{\nu_t(u) + k_t \Delta t}, \tag{31}$$

and

$$\boldsymbol{F}_s^+ = \frac{k_t \mu_m \|\boldsymbol{F}_n^c\| \dfrac{\boldsymbol{F}_s^{e+}}{\|\boldsymbol{F}_s^{e+}\|} \Delta t + \nu_t(u)\left(\boldsymbol{F}_s^- - k_t \dot{\boldsymbol{v}}_s \Delta t\right)}{\nu_t(u) + k_t \Delta t}. \tag{32}$$

Further substitution and factorization by $\boldsymbol{F}_s^{e+}$ gives a more compact expression:

$$\boldsymbol{F}_s^+ = \boldsymbol{F}_s^{e+} \frac{\nu_t(u) + k_t \Delta t \mu_m \dfrac{\|\boldsymbol{F}_n^c\|}{\|\boldsymbol{F}_s^{e+}\|}}{\nu_t(u) + k_t \Delta t}. \tag{33}$$

2.3. Note on motion integration in DEM

The classical motion integration in DEM requires a single evaluation of the interaction forces at time t to compute positions and velocities at time $t + \Delta t$. This is done classically with a symplectic integrator using a centered, second order accurate, finite difference approximation of the translational and rotational accelerations. The details of this integration is beyond the scope of the paper yet an important feature is that it sets an upper bound to Δt for numerical stability, which has a critical influence on the total computation time (a detailed derivation can be found in [24]).

In brief the computational time-step for rate-independent (non-viscous) interactions depends on the incremental stiffness of each interaction, i.e. the partial derivatives of $\boldsymbol{F}$ with respect the particle positions.

For rate-dependent interaction models such as the LSD however, an additional stability condition appears in the viscosity dominated regimes, since the forces depend not only on positions but also on velocities. To avoid this constraint many authors tune the interaction viscosity in order to stick to the under-damped, elasticity dominated, regime. Obviously such a trick is not acceptable in a lubrication model, where fluid viscosity has to be taken for what it is.

A key feature of the visco-elastic interaction defined in previous sections is that it leaves the stability of explicit motion integration independent of viscosity ν, and even

of v/u. Indeed the stiffness g is an upper bound of the incremental stiffness regardless of other parameters (the upper bound being approached when viscosity dominates). In practice, it is thus enough to determine Δt using the same expressions as for rate-independent interactions, using g as the contact stiffness. It does not only make selecting the computational time-step straightforward, but also, and more importantly, it lets limit cases be approached with no impact on the computational cost (e.g. viscosity dominated regimes, perfectly smooth particles, vanishing gap distances...).

3. Test cases

In this section, two 2-spheres simulations are performed using the computational scheme introduced previously and the DEM code Yade-DEM. In this code, motion is integrated by a conventional explicit, 2nd order, central finite difference scheme. A link to the algorithm used to generate these test cases is provided in reference 25.

3.1. Falling sphere

In this first test case two immersed spheres undergo normal motion only. The simulation consists in one fixed sphere and one free sphere subjected to gravitational acceleration. The free sphere is initially static at position $(0, u_0, 0)$. The fixed sphere remains at position $(0, 0, 0)$. This test shows the robustness and numerical stability of the model down to very small gaps. Various regimes are expected depending on input parameters. When the viscosity is high enough, the trajectory is dominated by viscous effects and the gap distance tends to decay exponentially with time. If roughness is finite, the gap closure converges to a final value corresponding to static equilibrium, else it converges to zero. For less viscous situations, the trajectory may appear nearly parabolic in the early stage. However, viscosity will necessarily come into play when the spheres are close enough. Finally, the free sphere may bounce, oscillate around the static position, or approach it in over-damped mode.

[Figure 3 about here.]

The equation of motion for this system gives

$$\begin{cases} m\ddot{u}_n &= -mg - k_b u_e \\ m\ddot{u}_n &= -mg - k_n \max(0, \varepsilon a - u) - \frac{3}{2}\pi\eta_f a^2 \frac{\dot{u}}{u} \\ u_n &= u + u_e \end{cases} \tag{34}$$

This system is non-linear, and as far as we know, it cannot be solved analytically. However, it is still possible to obtain partial solutions with some simplifications. For quasi-static motion controlled by viscous damping and hard spheres ($u_e \to 0$), this system can be reduced to:

$$0 = -mg - \frac{3}{2}\pi\eta_f a^2 \frac{\dot{u}}{u}, \tag{35}$$

which has the solution

$$u = u_0 \exp\left(\frac{-8}{9}\frac{t}{\tau_c}\right), \tag{36}$$

where τ_c is the characteristic sedimentation time: $\tau_c = \eta_f / a\rho g$.

At static equilibrium, there must be a persistent contact through asperities (for finite roughness at least), with the normal force balancing weight, and all velocities must be null. The elastic displacement at equilibrium is thus given by

$$u_{eq} = \varepsilon a - \frac{mg}{k_n} \tag{37}$$

Note that this equilibrium does not exist for heavy yet soft particles, when $\epsilon a < mg/k_n$. In this case, the gap distance still decreases exponentially but it does so with an apparent weight reduced by the contact force corresponding to $u = 0$: $\boldsymbol{F}_n^c(u = 0) = -k_n \varepsilon a \boldsymbol{n}$.

The problem involves two dimensionless numbers, in addition to the relative roughness ϵ. Let us define the "contact number" $\mathcal{K}$, which balances the contact force and the particle weight at equilibrium, i.e.

$$\mathcal{K} = \frac{k_n \varepsilon}{\frac{4}{3}\pi a^2 \rho g} \tag{38}$$

This number can be generalized in the case of suspensions, as $\mathcal{K} = E\varepsilon/P_p$, where E is the particle elastic modulus and P_p the confining pressure applied on the particle phase. For the present test case, if the contact number goes below 1, there is no static equilibrium.

The other relevant number for this test case is the Stokes number, generally defined as $\mathcal{S}t = a\rho\dot{u}/\eta_f$. Since the characteristic velocity for this problem is the undamped free-fall velocity, $\dot{u}^2 = 2u_0 g$, the Stokes number reads

$$\mathcal{S}t = \frac{a\rho\sqrt{2u_0 g}}{\eta_f} \tag{39}$$

When the Stokes number is small enough, the trajectory is driven by viscous effects, as in over-damped oscillators. In contrast, if this number is high, the sphere should collide as in a nearly undamped, or under-damped, oscillator.

[Figure 4 about here.]

Figure 4 shows several typical solutions of this test case. The initial trajectory is always dominated by gravity since viscous forces are initially null (no initial velocity), which results in a quadratic evolution of position with time just after the start. Then, for rigid particles or smooth particles at low Stokes numbers, the movement is damped (a), and the falling sphere reaches static equilibrium smoothly. With soft particles, the trend is for the free sphere to be entrapped by lubrication (b), as if the surfaces where sticking. The oscillations in u are so small that viscous dissipation becomes negligible, hence the center of mass keeps oscillating in a nearly undamped mode. For high Stokes number as in (c), the rebound energy is sufficient for the sphere to detach after the collisions and we recover damped bouncing. Note that the restitution coefficient progressively decreases at each bouncing, and the number of bouncing is finite. Situation (a) can be seen as the last rebound of a series starting like (c). Finally, (d) is intermediate between (b) and (c), the stiffness is small enough to enable oscillations but still high enough for bouncing.

[Figure 5 about here.]

The three dimensionless numbers (ε, $\mathcal{K}$, and $\mathcal{S}t$) have been investigated in an extensive set of simulations in order to obtain a complete phase diagram of the type of response (damping, bouncing, oscillating). The complete phase diagram is a volume and some slices for $\mathcal{S}t$ from 10 to 10^4 are presented in figure 5. As showed in figure 4d, simulations close to the transitions exhibits both behaviours. Then, the transition

between areas are smooth rather than sharp. For the highest Stokes simulations (a), the trajectories exhibit mainly either oscillating or bouncing according to the particles stiffness. The softest ones ($\mathcal{K} < 0.7$) are oscillating after first collision whereas the stiffest ones bounces. Even at this Stokes number, there are still some parameters where the ideal exponential damping predicted by equation 36 is recovered. Reducing the Stokes number (from (a) to (d)) let more and more configurations being damped, but only for stiff cases. The oscillating area is being affected for lower Stokes number (e,f).

When the Stokes number is small enough, all trajectories are completely driven by viscous forces, and the solution calculated in (36) is recovered until the two spheres create a contact. Figure 6a shows it is indeed the case down to very small gaps for smooth particles. For rough particles, this solution is also obtained before reaching contact. Rough particles with negative equilibrium distances u_{eq} exhibit an exponential behaviour with a longer characteristic time associated to the apparent weight discussed above. As shown in Figure 6c an excellent agreement is found between the gap reached at the end of the simulation and the calculated equilibrium one.

[Figure 6 about here.]

To conclude, this first test case enables to verify the implementation of the method by comparing the numercial solution to the analytical one at low Stokes number for both rough and smooth spheres. It also highlights that for the latter, it is robust down to arbitrary small gaps.

3.2. Two spheres in a shear flow

[Figure 7 about here.]

[Figure 8 about here.]

The second test case concerns the motion of two neutrally buoyant spheres suspended in a sheared fluid. This problem has been studied extensively by numerical methods and compared to closed-form solutions in earlier works [26, 6, 7, 27, 28]. The closed-form solutions come from analytical integration of Stokes' equations in linear flow fields [29, 30], of which shear flow is a particular case [31, 32].

The spheres are subjected to entrainment by the suspending fluid, and lubrication forces as they approach each other. The entrainment is modelized by Stokes drag, for which force F^d and torque T^d are given by

$$\boldsymbol{F}^d = -6\pi\eta_f a\left(\dot{\boldsymbol{r}} - \boldsymbol{w}_f\right) \tag{40}$$

$$\boldsymbol{T}^d = -8\pi\eta_f a^3\left(\boldsymbol{\omega} - \frac{1}{2}\nabla\times\boldsymbol{w}_f\right) \tag{41}$$

where $\boldsymbol{w}_f$ is the background fluid velocity given by $(\dot{\gamma}y;\, 0;\, 0)$, $\dot{\boldsymbol{r}}$ and $\boldsymbol{\omega}$ are the particle velocity and spin velocity, respectively. The initial particle positions are $(0, 0, 0)$ and $(-10a, d_0\sin\theta, d_0\cos\theta)$, with initial velocity and spin corresponding to the force and torque free case in the above equations. All distances are normalized by a and noted with "*" for the comparison with analytical results. Besides θ and d_0/a, the relevant dimensionless numbers of the problem are the roughness and the ratio of viscous stress to stiffness: $\eta_f\dot{\gamma}/E$. This last number controls the deformation of the sphere induced by viscous forces. Examples of soft systems for which this coupling has been studied include bubbles, drops, vesicles or elastic capsules, for which the stiffness is an interfacial property (surface tension or surface modulus). By analogy to these cases and similarly to other authors (see e.g. reference 33), let us call the above number the Capillary Number, $Ca = \eta_f\dot{\gamma}/E$.

Whereas suspended smooth hard spheres follow reversible paths, both roughness (i.e. the possibility of solid contact) and deformability of the particles are known to induce non reversible, the particles being driven to different streamlines as a result of the interaction [31, 34]. Figure 8 illustrates this three typical cases: smooth hard spheres, rough hard shperes, deformable particles.

[Figure 9 about here.]

The case of smooth hard spheres is particularly interesting since it can be directly compared to the analytical solution of Da Cunha and Hinch [31]. As it can be seen on figure 8a, the obtained trajectories follow the analytical solutions from Da Cunha and Hinch [31] for smooth hard spheres with a maximum deviation of 2%. However, looking into details to the gap between the spheres, a discrepancy could be detected between the numerical and the analytical one. Although it has no consequences on the

trajectories, it is interesting to discuss its origin. In the numerical model, the fluid is accounted by a combination of Stokes drag and lubrication force and torque. As stated in the model description, the lubrication analytical expressions are only valid for small gaps, and are set to zero in the model when the gap exceeds an arbitrary distance. We have varied this lubrication cut off distance from $2a$ to $7a$. The results are displayed in Fig 9, in terms of the minimal gap reached during the simulation. Clearly, this cut off has a rather strong influence on this minimal gap - although the trajectories remain nearly unchanged overall. A larger cur-off distance tends to increases the minimal gap, the best match to the analytical solution of Da Cunha and Hinch [31] being obtained at $4a$. This cut-off value was thus retained since there was no other objective way to define it, and the minimal distance was somehow sensitive to it. That the same cutoff should be used in all cases is no implied since the two-sphere system is not representative of typical applications. The influence of the cut-off distance is much smaller when simulating dense or, even, semi-dilute suspensions. The dominant lubrication terms are indeed due to the nearest neighbours in general, and the nearest neighbours are generally much closer than $4a$. Any cut-off value beyond one particle diameter will lead to quantitatively similar results.

The very good agreement between with the analytical solution for smooth hard sphere is interesting as it clearly shows that lubrication forces and torques are sufficient to describe the viscous interaction between two spheres. This conclusion differs to the one which is mentioned in Metzger et al. [26], where a significant discrepancy is found between the numerical solution obtained with lubrication interaction and the analytical solution. This has been interpreted as the consequence of neglecting the long-range interaction which are present the Stokes equation. In fact, in reference 26, only the normal component of the lubrication force was considered; additionally no drag torque was considered. By turning off tangential forces or sphere rotation, we indeed obtain a similar discrepancy with the analytical solution , as shown in figure 10. This consideration allows us to highlight that tangential lubrication forces are crucial to get quantitative results - they are too often neglected in numerical models. The cost of computing the shear component in the present model is small compared to the normal component and it does not introduce additional constraints in terms of numerical

stability. Therefore there is no substantial computational gain to expect by neglecting these terms - besides the fact that ignoring them would make the model quantitatively wrong.

[Figure 10 about here.]

A set of typical trajectories for rough stiff spheres is presented in figure 8b. As expected, roughness breaks the symmetry as soon as contact occurs. The role of roughness is apparent in the plots of u^*, which look as if the smallest distances were truncated. The sphere then moves to a streamline corresponding to $\min(u^*) \approx \varepsilon$ irrespective of the initial position of the particle. As seen in figure 9 for smooth spheres ($\varepsilon = 0$), u^* reaches a finite minimum value when $d_0^* \to 0$, and this distance is about $3\ 10^{-5}$. Consistently, the results are not modified by a finite roughness as long as $\varepsilon < 3\ 10^{-5}$.

Another set of trajectories is presented for soft spheres in figure 8c. Up to our knowledge, there is no analytical solution in that case. However, changes of streamline have been reported in the literature, based on experiments and on simulations [34]. The trajectories with large capillary number are qualitatively similar to those found in the literature. A noticeable effect is that the closure of the gap is smaller as compared to stiff spheres, which implies - for a given value of roughness - a smaller normal contact force and therefore a lower resistance to contact sliding.

[Figure 11 about here.]

We have performed a systematic analysis of the streamline deviation, varying both roughness and capillary numbers. The results are summarized in figure 11, which reports the magnitude of the streamline deviation for almost coaxial initial distances ($d_0^* = 10^{-2}$) For this kind of initial separation distance, the streamline is very close from the closed-loop streamline border for smooth hard spheres. Therefore, if any streamline deviation occurs, the far deflection gives the height of an area that is not reachable anymore after spheres interaction. The red area highlights the cases where this distance is strictly 0. It approximately corresponds to cases where $\varepsilon < 3\times10^{-5}$ and $Ca < 10^{-4}$. From this figure, we can deduce the main origin of irreversibility above these limits. When $\varepsilon \gg Ca$, the streamline deviaton is controlled by the roughness,

whereas when $Ca \gg \varepsilon$, it is controlled by the particle deformation. Strikingly, when Ca and ε are of the same order of magnitude, the streamline deviation is smaller than the case of rigid particles of similar roughness or than the case of smooth deformable particles. This non-monotonic effect is probably due to the fact that the particle stiffness also controls the deformation of the roughness. In case of intermediate roughness and capillary numbers, the apparent roughness is smaller than at low Ca.

To conclude, this test case shows that the model reproduces very well analytical results in the case of rigid particles. Extension to slightly deformable particles allow to predict the existence of reversible trajectories at low Ca and for rather smooth particles. It also lead to a phase diagram of the origin of irreversibility.

4. Conclusion

A complete model of lubricated contact and an unconditionally stable integration scheme for the interaction forces have been introduced in section 2. The model can be readily implemented as an interaction model in conventional granular simulations. The scheme handles the case $\varepsilon = 0$ (perfectly smooth spheres) gracefully, and regularization by elasticity removes the singularity of lubrication when $u \to 0^+$. Furthermore the visco-elastic coupling is such that the stability of explicit integrator for particle dynamics is independent of viscous terms, whereas viscosity dominated regimes were challenging most explicit schemes until now.

This work contributed an implementation in the open source discrete element code Yade-DEM.org [35] (used for running the test cases of last section). The lubricated contact model presented here is available as part of that code and our results can be reproduced independently.

Two test cases have been investigated. The first one evidenced the robustness of the method. In the viscous regime, the decreasing exponential trajectory has been recovered. In the regime where inertia is not negligible, some behaviours like damped bouncing (close to pure-elastic limit) and vibration after collision (soft limit) have been reproduced by the model. Two dimensionless numbers are shown to control the response in that simple two-sphere system, and a phase diagram is proposed, showing

the interplay between stiffness, roughness and viscosity. These dimensionless numbers might bear some relevance to shear flows of granular suspensions.

The second test case, two spheres suspended in a sheared liquid, has been extensively used to compare models and theories. We found a good agreement with theoretical solutions for stiff spheres, and we reproduced qualitatively some features observed previously with soft particles. A phase diagram has been determined concerning the deviation from reversible trajectories in shear flows, which originates either from particle roughness, either from particle deformation.

Acknowledgements

The authors acknowledge Univ. Grenoble Alpes for financial support. 3SR and LRP are members of Labex Tec21, and LRP of Institut Carnot Polynat. Computations presented in this paper were performed using the CIMENT infrastructure (`https://ciment.ujf-grenoble.fr`), which is supported by the Rhône-Alpes region (GRANT CPER07_13 CIRA: `http://www.ci-ra.org`).

Notations

[Table 1 about here.]

[1] J. J. Stickel, R. L. Powell, Fluid mechanics and rheology of dense suspensions, Annu. Rev. Fluid Mech. 37 (2005) 129–149.

[2] J. F. Morris, A review of microstructure in concentrated suspensions and its implications for rheology and bulk flow, Rheol. acta 48 (2009) 909–923.

[3] C. Thornton, Z. Ning, A theoretical model for the stick/bounce behaviour of adhesive, elastic-plastic spheres, Powder Technology 99 (1998) 154 – 162.

[4] C. Thornton, Granular dynamics, contact mechanics and particle system simulations, Springer, 2015.

[5] F. Peters, G. Ghigliotti, S. Gallier, F. Blanc, E. Lemaire, L. Lobry, Rheology of non-brownian suspensions of rough frictional particles under shear reversal: A numerical study, J. Rheol. 60 (2016) 715–732.

[6] K. Yeo, M. R. Maxey, Simulation of concentrated suspensions using the force-coupling method, J. Comp. Phys. 229 (2010) 2401 – 2421.

[7] S. Gallier, E. Lemaire, L. Lobry, F. Peters, A fictitious domain approach for the simulation of dense suspensions, J. Comp. Phys. 256 (2014) 367 – 387.

[8] A. Vázquez-Quesada, M. Ellero, Rheology and microstructure of non-colloidal suspensions under shear studied with smoothed particle hydrodynamics, J. Non-Newton. Fluid 233 (2016) 37 – 47.

[9] H. Tanaka, T. Araki, Simulation method of colloidal suspensions with hydrodynamic interactions: Fluid particle dynamics, Phys. Rev. Lett. 85 (2000) 1338–1341.

[10] B. Van den Brule, R. Jongshaap, Modeling of concentrated suspensions, J. Stat. Phys. 62 (1991) 1225–1237.

[11] R. Ball, J. R. Melrose, A simulation technique for many spheres in quasi-static motion under frame-invariant pair drag and brownian forces, Physica A 247 (1997) 444–472.

[12] R. Mari, R. Seto, J. F. Morris, M. Denn, Shear thickening, frictionless and frictional rheologies in non-brownian suspensions, J. Rheol. 58 (2014) 1693.

[13] D. Marzougui, B. Chareyre, J. Chauchat, Microscopic origin of shear stress in dense fluid-grain mixtures, Granular Matter 17 (2015) 297–309.

[14] S. Gallier, F. Peters, L. Lobry, Simulations of sheared dense noncolloidal suspensions: Evaluation of the role of long-range hydrodynamics, Phys. Rev. Fluids 3 (2018) 042301.

[15] W. Chèvremont, B. Chareyre, H. Bodiguel, Quantitative study of the rheology of frictional suspensions: Influence of friction coefficient in a large range of viscous numbers, Phys. Rev. Fluids 4 (2019) 064302.

[16] Y. Zhao, R. H. Davis, Interaction of two touching spheres in a viscous fluid, Chemical Engineering Science 57 (2002) 1997 – 2006.

[17] J. Brändle de Motta, W.-P. Breugem, B. Gazanion, J.-L. Estivalezes, S. Vincent, E. Climent, Numerical modelling of finite-size particle collisions in a viscous fluid, Phys. Fluids 25 (2013) 083302.

[18] R. Seto, R. Mari, J. F. Morris, M. M. Denn, Discontinuous Shear Thickening of Frictional Hard-Sphere Suspensions, Phys. Rev. Lett. 111 (2013).

[19] M. Trulsson, B. Andreotti, P. Claudin, Transition from the viscous to inertial regime in dense suspensions, Phys. Rev. Lett. 109 (2012) 118305.

[20] O. R. Walton, R. L. Braun, Viscosity, granular-temperature, and stress calculations for shearing assemblies of inelastic, frictional disks, J. Rheol. 30 (1986) 949.

[21] P. Cundall, O. Strack, Discrete numerical-model for granular assemblies, Geotechnique 29 (1979) 47–65.

[22] N. Frankel, A. Acrivos, On the viscosity of a concentrated suspension of solid spheres, Chem. Eng. Sci. 22 (1967) 847–853.

[23] D. Jeffrey, Y. Onishi, The forces and couples acting on two nearly touching spheres in low-reynolds-number flow, Zamm-Z Angew. Math. Me. 35 (1984) 634–641.

[24] R. A. Hosn, L. Sibille, N. Benahmed, B. Chareyre, Discrete numerical modeling of loose soil with spherical particles and interparticle rolling friction, Granular Matter 19 (2017) 4.

[25] W. Chèvremont, Code used to generate test cases, `https://gitlab.com/yade-dev/trunk/tree/master/examples/Lubrication`, 2019.

[26] B. Metzger, P. Pham, J. Butler, Irreversibility and chaos: Role of lubrication interactions in sheared suspensions, Phys. Rev. E 87 (2013) 052304.

[27] J. Kromkamp, D. van den Ende, D. Kandhai, R. van der Sman, R. Boom, Lattice boltzmann simulation of 2d and 3d non-brownian suspensions in couette flow, Chem. Eng. Sci. 61 (2006) 858 – 873.

[28] S. Gallier, E. Lemaire, F. Peters, L. Lobry, Rheology of sheared suspensions of rough frictional particles, J. Fluid Mech. 757 (2014) 514–549.

[29] G. K. Batchelor, J. T. Green, The hydrodynamic interaction of two small freely-moving spheres in a linear flow field, J. Fluid Mech. 56 (1972) 375–400.

[30] T. van de Ven, S. Mason, The microrheology of colloidal dispersions: Iv. pairs of interacting spheres in shear flow, J. Colloid Interf. Sci. 57 (1976) 505 – 516.

[31] F. R. Da Cunha, E. J. Hinch, Shear-induced dispersion in a dilute suspension of rough spheres, J. Fluid Mech. 309 (1996) 211–223.

[32] C. J. Lin, K. J. Lee, N. F. Sather, Slow motion of two spheres in a shear field, J. Fluid Mech. 43 (1970) 35–47.

[33] T. Gao, H. H. Hu, Deformation of elastic particles in viscous shear flow, J. Comp. Phys. 228 (2009) 2132 – 2151.

[34] E. Lac, A. Morel, D. Barthès-Biesel, Hydrodynamic interaction between two identical capsules in simple shear flow, J. Fluid Mech. 573 (2007) 149–169.

[35] V. Šmilauer, et al., Yade Documentation 2nd ed, The Yade Project, 2015.

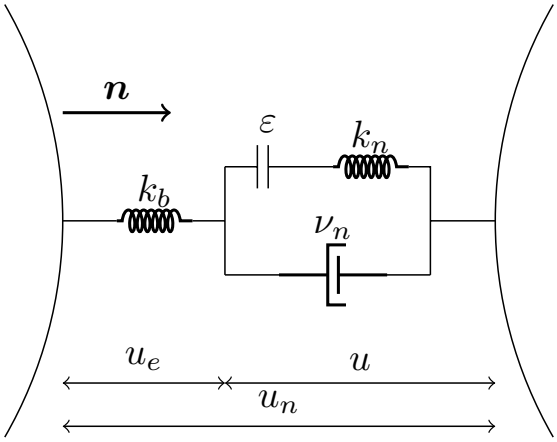

Figure 1: Rheological scheme for normal component.

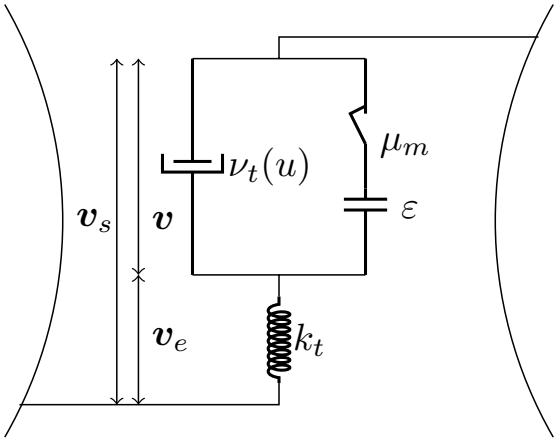

Figure 2: Rheological scheme for the tangential component.

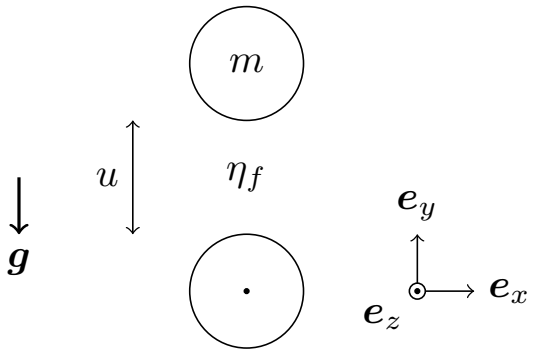

Figure 3: Representation of falling sphere test case

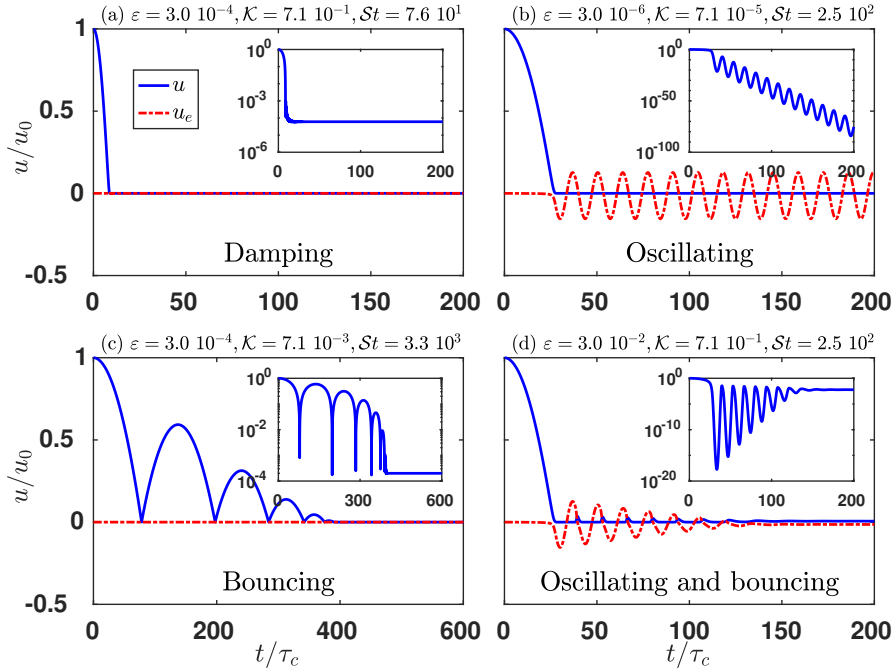

Figure 4: Typical solutions for free-falling spheres. *(a)* Damped solution with inertial starts, *(b)* Oscillating solution, *(c)* Bouncing solution, *(d)* Mixed boucing and oscillating solution. Inserts shows the gap u in log scale.

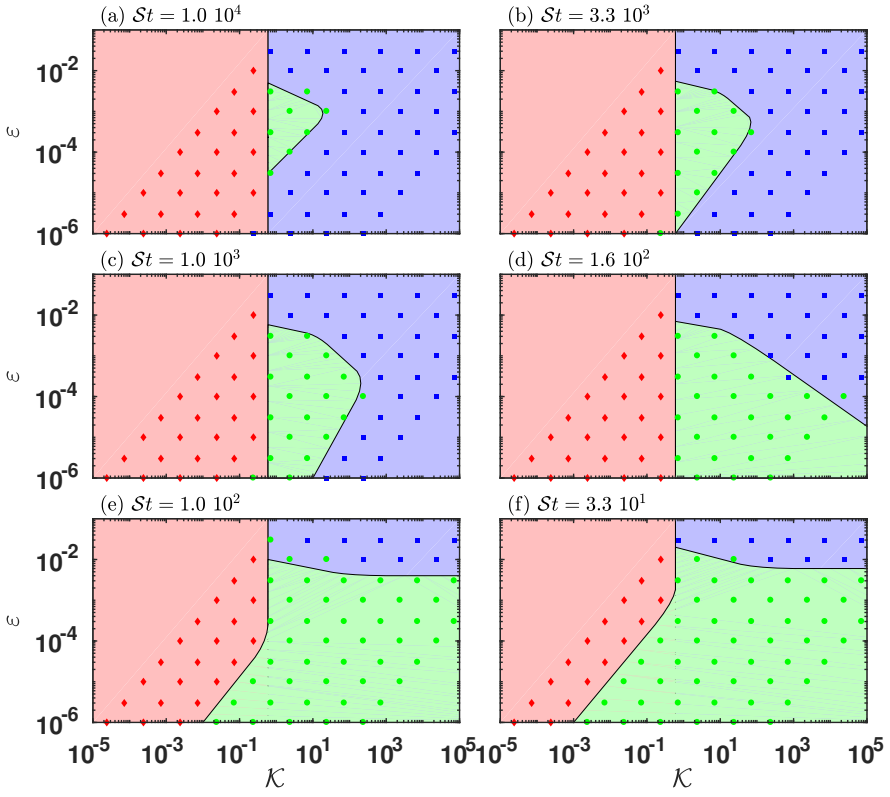

Figure 5: Slices of phase diagram at several values of $\mathcal{S}t$. Oscillations are in red ($\diamond$), Bouncing are in blue ($\square$), Damped are in green ($\circ$). Points shows simulation data in that plane. Borders are determined from complete set of data (in $3D$), then smoothed and sliced to obtain these figures.

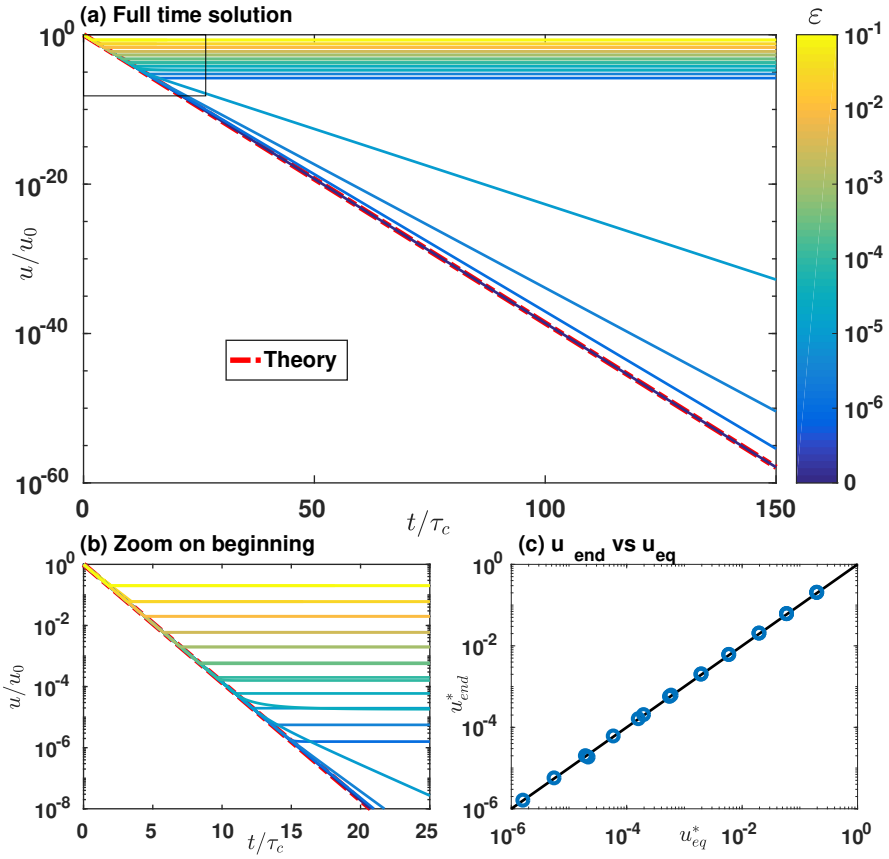

Figure 6: Results of simulations for various parameters. $\mathcal{S}t \in [10^{-6} - 10^{-2}], \varepsilon \in [0; 10^{-6} - 10^{-1}]$. Dashed dotted curve (.-) is the smooth solution, given equation 36. Line colors indicate the value of ε. The curves obtained with different Stokes numbers but with the same roughness superimpose in the range tested. (a) Solution for the full time range of simulation. (b) Magnified view of the data shown in (a). (c) Comparison between theoretical and numerical equilibrium distances. Relative difference between the obtained equilibrium and theoretical equilibrium is $|1 - u_{end}/u_{eq}| < 10^{-8}$.

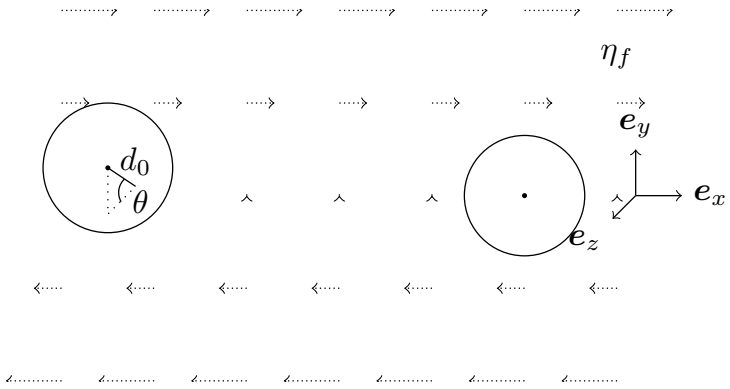

Figure 7: Scheme of the test case: two spheres in a shear flow.

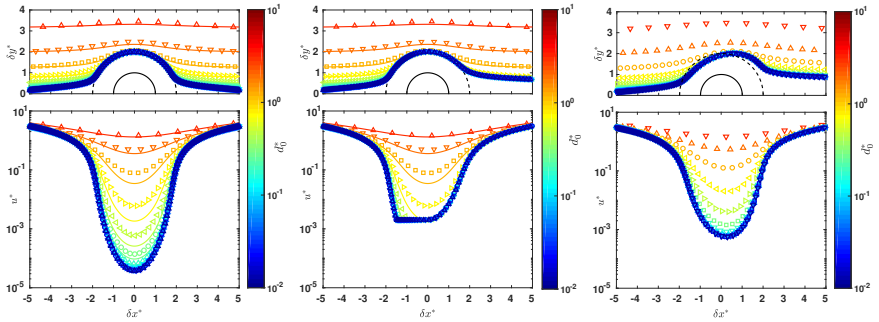

(a) Smooth ($\varepsilon = 0, Ca = 10^{-6}$) (b) Rough ($\varepsilon = 2\ 10^{-3}, Ca = 10^{-6}$) (c) Soft ($\varepsilon = 0, Ca = 10^{-2}$)

Figure 8: Relative trajectories of spheres, computed by DEM (points) and compared to Da Cunha and Hinch [31] solution (solid lines), in the shear/velocity plane ($\theta = \pi/2$). The black half-circles represents the sphere on which the relative trajectory is computed (solid lines) and the limit trajectory for hard spheres (dashed lines).

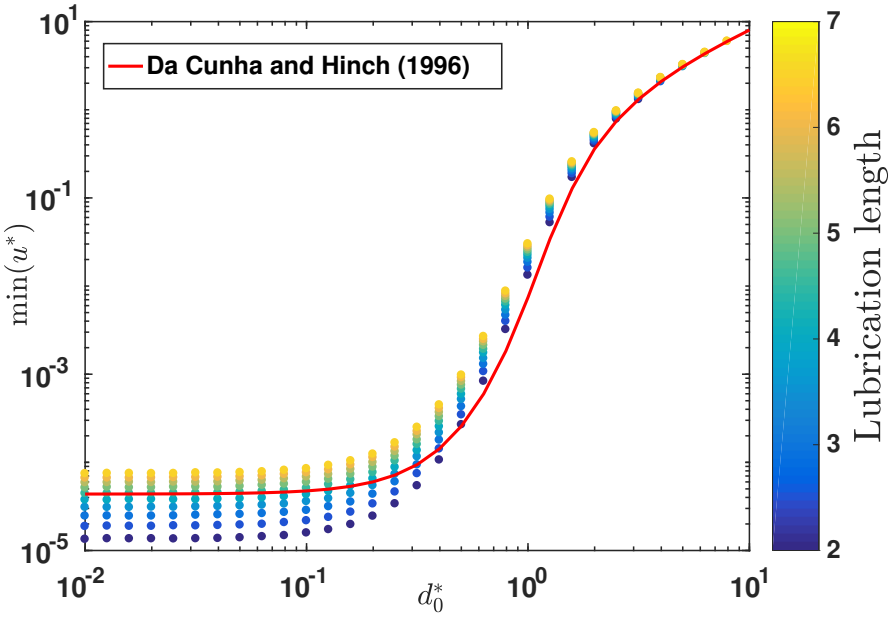

Figure 9: The minimum separation from DEM and Da Cunha and Hinch [31] versus initial separation and cut-off distance of lubrication, particles centers are in the shear/velocity plane ($\theta = \pi/2$). Lubrication length is the distance from which the lubrication is taken into account.

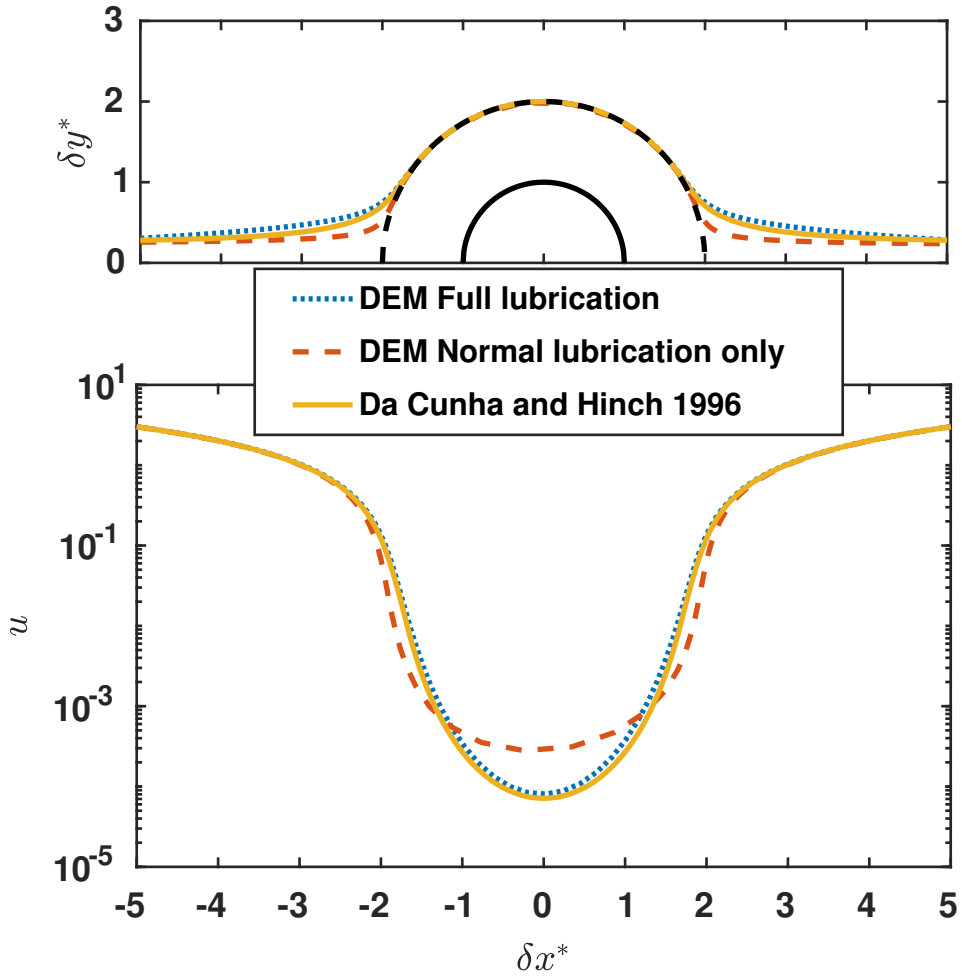

Figure 10: Comparison of trajectories and distances obtained with all components of lubrication, with normal lubrication only and compared to the analytical solution of Da Cunha and Hinch [31].

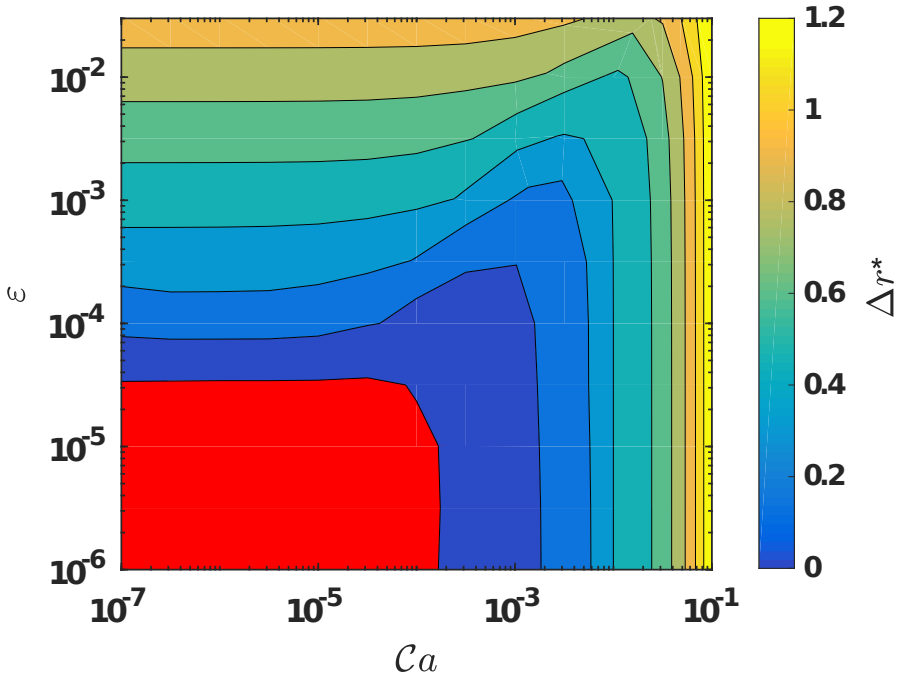

Figure 11: Map of streamline deviation as function of roughness and capillary number. In the red area, the streamline change is strictly 0.

a	Mean particles radius
d_0	Initial streamline separation distance
E	Elastic modulus
$\boldsymbol{F}$	Force
g	Gravity
k_b	Bulk normal stiffness
k_n	Roughness stiffness
k_t	Bulk tangential stiffness
m	Mass
$\boldsymbol{n}$	Normal vector
P_p	Particules confining pressure
$\boldsymbol{r}$	Sphere position
$\boldsymbol{T}$	Torque
t_c	Critical collision time
u	Distance between deformed surfaces
u_0	Initial distance between spheres
u_e	Surface deflection
u_{eq}	Equilibrium distance between deformed spheres
u_n	Geometrical overlap between spheres
$\boldsymbol{v}$	Plastic slip
$\boldsymbol{v}_e$	Elastic tangential displacement
$\boldsymbol{v}_s$	Integral of total tangential displacement
$\boldsymbol{w}_f$	Flow field
α	Roughness to bulk stiffness ratio
$\dot{\gamma}$	Shear rate
Δt	Timestep
ε	Relative roughness
η_f	Fluid viscosity
θ	Angle
μ_m	Friction coefficient
ν_n	Prefactor for normal lubrication
ν_t	Prefactor for tangential lubrication
ξ	Logarithm of u/a
ρ	Density
τ	Viscoelastic characteristic time
τ_c	Sedimentation characteristic time
$\boldsymbol{\omega}$	Sphere's rotations
$\mathcal{C}a$	Capilary number
$\mathcal{K}$	Contact number
$\mathcal{S}t$	Stokes number
$\cdot^c$	Contact
$\cdot^d$	Drag
$\cdot_i$	Intermediate result
$\cdot^l$	Lubrication
$\cdot_n$	Normal component
$\cdot_r$	Roll component
$\cdot_s$	Tangential component
$\cdot_t$	Twist component
$\cdot^*$	Dimensionless component
$\cdot^+$	Variable at current timestep
$\cdot^-$	Variable at previous timestep

Table 1: Notations used